

Laser-thinning of MoS₂: on demand generation of a single-layer semiconductor

*A. Castellanos-Gomez**, *M. Barkelid*, *A. M. Goossens*, *V. E. Calado*, *H. S. J. van der Zant* and
*G. A. Steele**.

Kavli Institute of Nanoscience, Delft University of Technology, Lorentzweg 1, 2628 CJ Delft,
The Netherlands.

a.castellanosgomez@tudelft.nl , g.a.steele@tudelft.nl

Single-layer MoS₂ is an attractive semiconducting analogue of graphene that combines high mechanical flexibility with a large direct bandgap of 1.8 eV. On the other hand, bulk MoS₂ is an indirect bandgap semiconductor similar to silicon, with a gap of 1.2 eV, and therefore deterministic preparation of single MoS₂ layers is a crucial step towards exploiting the large direct bandgap of monolayer MoS₂ in electronic, optoelectronic, and photovoltaic applications. Although mechanical and chemical exfoliation methods can be used to obtain high quality MoS₂ single-layers, the lack of control in the thickness, shape, size, and position of the flakes limits their usefulness. Here we present a technique for controllably thinning multilayered MoS₂ down to a single-layer two-dimensional crystal using a laser. We generate single layers in arbitrary shapes and patterns with feature sizes down to 200 nm, and show that the resulting two-dimensional crystals have optical and electronic properties comparable to that of pristine exfoliated MoS₂ single layers.

Among two-dimensional crystals obtained by exfoliation of layered 3D materials,¹ graphene is by far the most studied due to its outstanding mechanical² and electronic properties.³ Other 2D crystals, however, have recently gained considerable interest, since their properties are complementary to those of graphene.⁴⁻⁸ For instance, the lack of a bandgap in graphene, which yields small current on/off ratios in graphene-based field effect transistors (FETs), has motivated research in other 2D semiconductor crystals such as MoS₂, which possess a large intrinsic bandgap.⁹

While in its bulk form, MoS₂ is an indirect gap semiconductor with a 1.2 eV bandgap; monolayer MoS₂ on the other hand has a direct gap of 1.8 eV.¹⁰ This indirect-to-direct transition, arising from quantum confinement effects as the thickness decreases,¹¹ results in an enhancement of the photoluminescence of monolayer MoS₂ with respect to the multilayered counterpart.¹²⁻¹⁵ Additionally, transistors based on single-layer MoS₂ present large in-plane mobilities (200-500 cm²V⁻¹s⁻¹) and high current on/off ratios (exceeding 10⁸)¹⁶ which make this

material of great interest for electronic devices and sensors.¹⁷⁻¹⁹ The excellent mechanical properties of MoS₂ also suggest its prospective use in flexible semiconducting applications.^{20, 21}

Until now, production of monolayer MoS₂ has been mainly performed by mechanical and chemical exfoliation of single layers from bulk crystals.^{1, 4, 12, 22} Although these exfoliation methods have proven to be effective to obtain high-quality MoS₂ single layers suitable for fundamental research, future applications require the development of new procedures to allow "on-demand" fabrication/modification of this nanomaterial.

Here, we present a top-down approach to fabricate MoS₂ single layers based on laser-thinning of multilayered MoS₂ flakes. The fabricated MoS₂ monolayers have been characterized by optical microscopy, atomic force microscopy (AFM) and Raman spectroscopy. In order to gain a deeper insight into their semiconducting properties, their photoluminescence (PL) spectra and their performance as a channel in FETs were explored. We find that laser-thinning of multilayered MoS₂ provides a reliable method to fabricate MoS₂ single layers with user-defined shape and size and with optical and electronic properties that are comparable to those of pristine MoS₂ single layers. The technique presented here offers the possibility to scale up the fabrication of single layer MoS₂.

In a typical experiment, a multilayered MoS₂ flake was deposited onto a Si/SiO₂ (285 nm) substrate by mechanical exfoliation¹ and characterized by a combination of optical microscopy, AFM and Raman spectroscopy (see Materials and Methods section). Figure 1(a) shows an optical micrograph of a multilayered MoS₂ flake on a Si/SiO₂ substrate. The regions with different color correspond to zones of the flake with different number of layers^{23, 24}, with the faint purple region in the center of Figure 1(a) corresponding to a single layer MoS₂.

A scanning laser from a confocal Raman microscope (Renishaw in via RM 2000, $\lambda = 514$ nm) was then used to thin the multilayered MoS₂ down to a monolayer by moving the laser over the flake with high power (see Materials and Method section for more details), in a similar way to the procedure employed to locally oxidize graphene or reduce graphene oxide²⁵⁻²⁷. We decided to employ a Raman system to perform the laser-thinning because it allows us to characterize *in situ* the Raman spectra and the optical contrast before and after the thinning procedure. This thinning procedure, however, can be implemented in other setups such as laser pattern generators which are optimized to perform fast laser-based lithography.

Figure 1(b) shows an optical micrograph of the same flake as in Figure 1(a) after the laser-thinning process in the region marked by the dotted rectangle in Figure 1(a). The optical contrast of the thinned region is uniform and consistent with that of a single MoS₂ monolayer^{23, 24}. The topography of the region thinned with the laser has been studied with AFM (Figure 1(c)). As can already be inferred from the contrast in the optical image, the initially multilayered MoS₂ flake has not been completely removed by the laser. Instead, a single layer of material with a thickness of 0.9 ± 0.3 nm remains on the surface, a value consistent with the expected thickness from a MoS₂ monolayer.

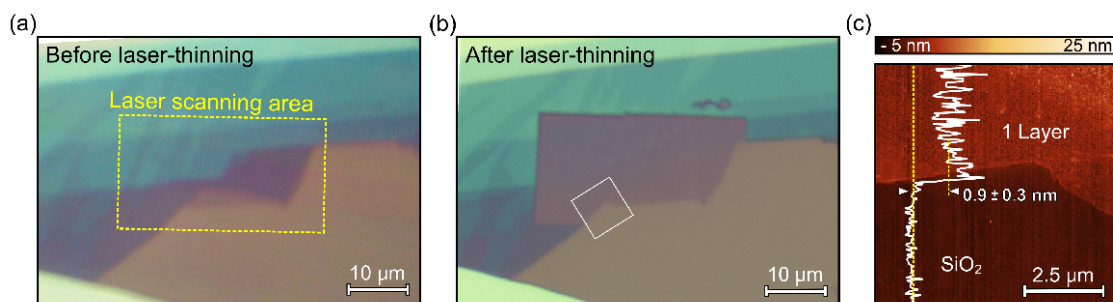


Figure 1. (a) Optical microscopy image of a multilayered MoS₂ flake deposited onto a 285 nm SiO₂/Si substrate. (b) Same as in (a) after scanning a laser in the area marked by a dashed rectangle in (a). The laser-thinning parameters were $\lambda = 514$ nm, incident power on the sample 10 mW, scan step 400 nm and exposure time of 0.1 sec between steps. (c) Topographic AFM images of the region marked by the square in (b). A vertical topographic line profile is included in (c) to indicate the thickness of the laser-thinned layer.

The thinning procedure relies on the sublimation of the upper layers due to the heating induced by light absorption. Apparently the heat cannot be easily dissipated through the substrate because of the poor coupling between the MoS₂ layers mediated by van der Waals forces. The bottom layer, however, remains on the substrate until much higher laser powers because it is in intimate contact with the SiO₂/Si substrate which acts as a heat sink. Using our experimental setup, the laser-thinning method can produce 8 $\mu\text{m}^2/\text{min}$. of MoS₂ monolayer and thus it can be used to thin down large-area multilayer MoS₂ crystals as those grown by recently developed vapor-phase methods^{28, 29}. The roughness of the laser-fabricated layers, however, is about three times larger than that of a pristine MoS₂ monolayer, probably due to the presence of unremoved MoS₂ traces on the surface, something we expect can be optimized by adjusting the laser scanning parameters. In the following, we characterize these laser-fabricated MoS₂ monolayers, demonstrating that their optical and electronic properties are comparable to that of pristine single layers.

Similar to the case of graphene, Raman spectroscopy can be employed to characterize the thickness of MoS₂ nanolayers^{13, 30}. Using a low-power laser (<1 mW to avoid laser-heating effects³¹), the Raman spectra of the initial multilayered MoS₂ flakes have been measured (Figure 2(a)). As reported by Lee *et al.*³⁰, the frequency difference between the two most prominent Raman peaks depends monotonically on the number of MoS₂ layers (blue circles in Figure 2(b)). Figure 2(b) also compares the Raman spectra measured for a MoS₂ flake before (4 layers thick) and after laser-thinning. The intensity of both the E_{2g}¹ and A_{1g} peaks and their frequency difference are drastically reduced after the thinning process, which is in agreement with a reduction of the thickness. The frequency difference value, however, is slightly larger than the one measured for a pristine MoS₂ monolayer (red square in Figure 2(b)). We attribute this discrepancy to the presence of traces of unremoved MoS₂ on the surface of the laser-fabricated monolayer, which would slightly modify the frequency of the Raman modes. Indeed, Eda *et al.*¹² observed a similar effect in MoS₂ monolayers fabricated by chemical methods and they attributed the discrepancy in the Raman mode frequencies to local thickness variations.

Additionally, the absence of a peak around 820 cm⁻¹ (fingerprint associated with the oxidation of MoS₂ and the formation of MoO₃) in the Raman spectra serves as a first indication to point out that the MoS₂ surface is not affected by oxidation during the laser-thinning process (see Supporting Information)³². Additionally, photoluminescence and electronic transport measurements (described in the following) support the interpretation that laser fabricated MoS₂ monolayers presents a semiconducting and not an insulating behavior (as it would be expected for MoO₃).

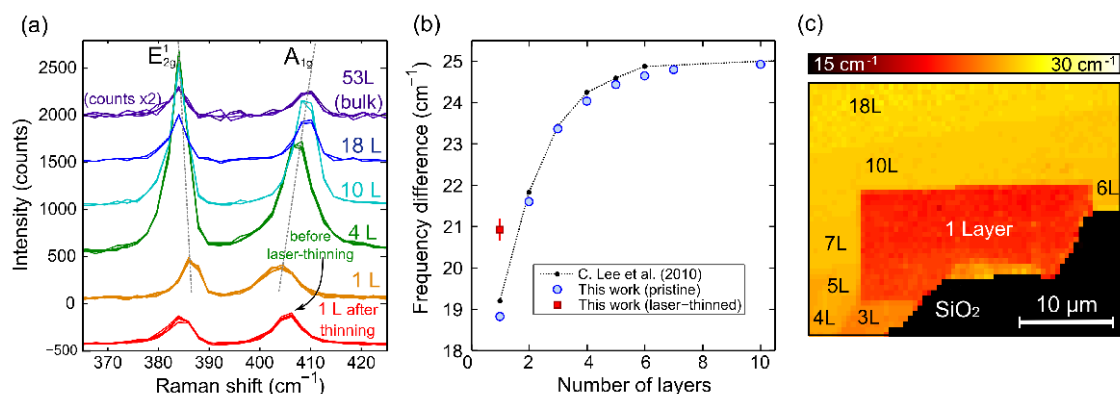


Figure 2. (a) Raman spectra of pristine MoS₂ flakes with thicknesses ranging from one single layer (1L) to 53 layers (53L). The spectrum measured for a laser-fabricated MoS₂ single layer is shown below the spectra for a pristine monolayer to facilitate the comparison. (b) Frequency difference between the E_{2g} and A_{1g} Raman modes. The red square represents the frequency difference measured for six laser-thinned MoS₂ monolayers. (c) Spatial map of the frequency difference between the Raman modes E_{2g} and A_{1g} measured in the laser-thinned flake shown in Figure 1b.

In addition to the Raman shift, single layer MoS₂ also exhibits a unique signature in its optical spectrum due to the transition from an indirect to a direct-bandgap semiconductor^{10, 12-15}. In Figure 3, we present the optical characteristics of our laser thinned MoS₂ layers. The PL signal of the initial 4-6 layers thick MoS₂ flake is rather weak in comparison to the PL spectrum of the pristine monolayer, in agreement with previous reports^{10, 15}. The PL spectrum of the laser-fabricated monolayer, however, resembles in intensity and frequency the one of the pristine MoS₂ monolayer, demonstrating that the laser-fabricated single layer MoS₂ also presents a large intrinsic direct bandgap (~1.8 eV), just as has been observed in mechanically exfoliated MoS₂ monolayers^{10, 15}. Figure 3(b) shows a false color image of the integrated PL signal measured in a region containing thinned and pristine zones. The laser-fabricated single layer MoS₂ can be clearly identified by the much more intense PL signal, shown as a brighter color in the image.

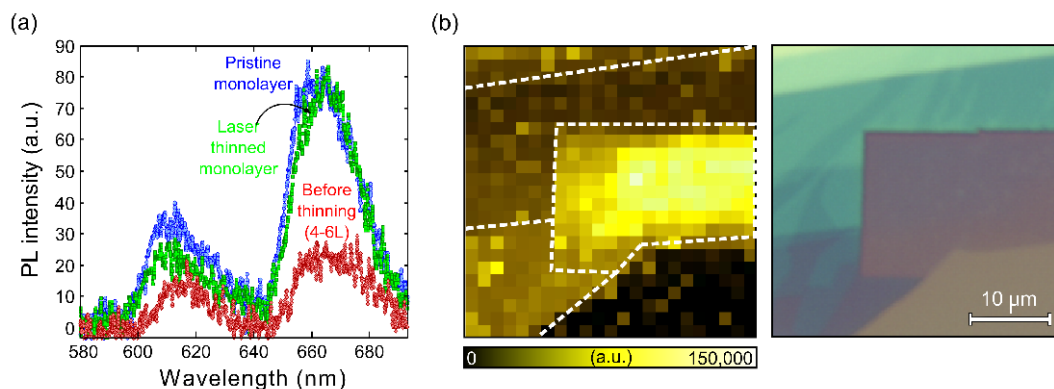


Figure 3. (a) Photoluminescence measured for a pristine monolayer, and for a 4-6 layers thick flake before and after laser-thinning. (b) A spatial map of the integrated photoluminescence signal between 580 nm and 700 nm, measured in the region indicated by the optical micrograph at the right. Dashed lines in PL image are a guide to the eye (extracted from the optical image shown on the right hand side) to identify the regions with different thicknesses in the MoS₂ flake.

To further compare the electrical properties of laser-fabricated and pristine MoS₂ monolayers, 11 FET devices (6 with laser-fabricated and 5 with pristine monolayers) were fabricated and characterized in two-terminal configuration. Figure 4(a) and 4(d) shows the optical micrographs of a pristine and a laser-fabricated single layer MoS₂ FET device respectively. The measured I_{ds} - V_g characteristics for both pristine and laser-fabricated samples (Figure 4(b) and 4(e)) are typical of an n-doped MoS₂ FET and in agreement with previous reports^{17, 24, 33, 34}. The current on/off ratio of both pristine and laser-fabricated devices is typically above 10^3 (for V_g ranging from -10 to 40 V), significantly higher than for graphene transistors. Figure 4(c) and (f) show the I_{ds} - V_{ds} characteristics for the pristine and laser-fabricated FETs at different gate voltages. While pristine monolayer-based FETs exhibit a saturating behavior, the current of laser-fabricated MoS₂ FETs does not saturate within the bias window studied here. It is important to note that similar non-saturating I_{ds} - V_{ds} characteristics have also been reported for pristine monolayer MoS₂-based FETs^{17, 24, 33, 34}. The origin of this non-saturating behavior is unknown.

The carrier mobility of the devices has been calculated from the following formula:

$$\mu = \frac{L}{W} \times \frac{d}{\epsilon_r \epsilon_0} \times \frac{\partial I_{ds}}{\partial V_g} \quad (1)$$

where L is the channel length, W is the channel width, ϵ_0 is $8.854 \cdot 10^{-12} \text{ F} \cdot \text{m}^{-1}$, ϵ_r is 3.9 for SiO₂ and d is the SiO₂ thickness (285 nm). We found that the mobility of laser-fabricated monolayers ($0.04 - 0.49 \text{ cm}^2 \text{V}^{-1} \text{s}^{-1}$) is comparable to that of pristine-monolayer based devices ($0.05 - 0.85 \text{ cm}^2 \text{V}^{-1} \text{s}^{-1}$), indicating the high quality of the laser-fabricated MoS₂ monolayers (see Supplementary Information for the characterization of all the fabricated devices). Although higher current on/off ratios and mobilities have been achieved in MoS₂ FETs with HfO₂-based top gates, due to the dielectric screening achieved with these high- κ gate dielectrics^{16, 18}, the

values obtained for our devices (including those based on laser-fabricated monolayers) are similar to previous studies on exfoliated MoS₂ FETs with a SiO₂-based backgate^{17, 24, 33, 34}.

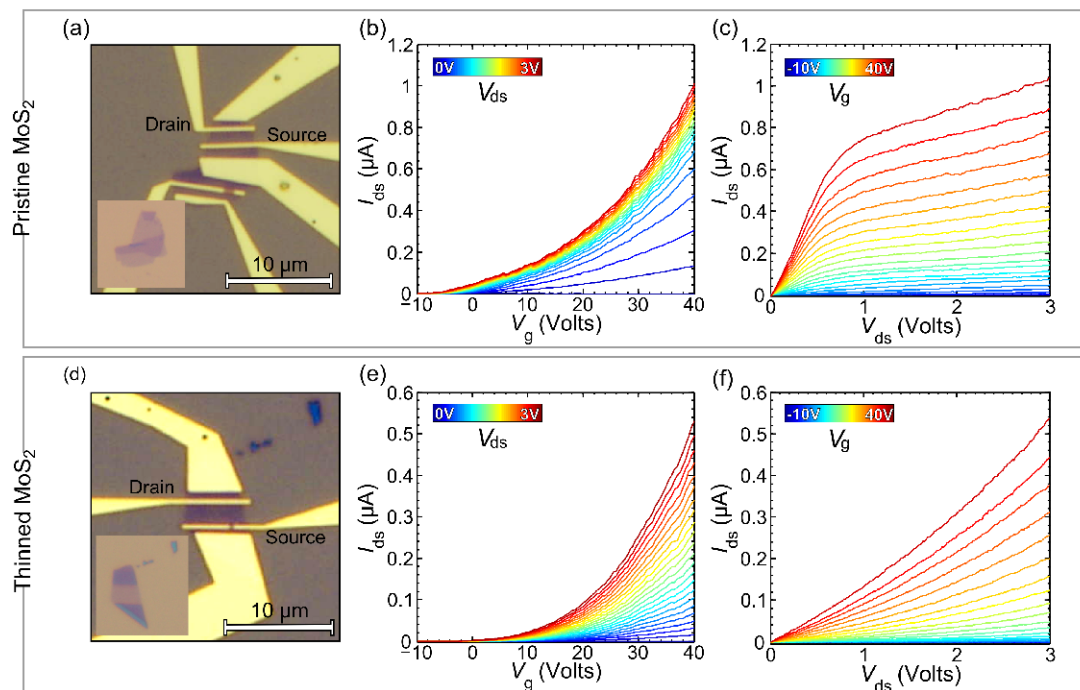


Figure 4. Optical micrographs of field effect transistors fabricated from a pristine MoS₂ monolayer (a) and a laser-fabricated monolayer (d). The insets in (a) and (d) show the MoS₂ flakes before processing. (b,e) Drain-source current as a function of gate voltage, measured for the pristine (b) and the laser-fabricated (e) MoS₂ FETs at different drain-source voltages. (c,f) Drain-source current as a function of the drain-source voltage, measure for different gate voltages, for the pristine (c) and the laser-fabricated (f) MoS₂ FETs.

Finally, we have further explored the possibility of employing this method to engineer the thickness of a multilayered flake following a desired pattern or even to completely cut through the flake. As the MoS₂ band structure depends on the number of layers, the control over the thickness allows to fabricate devices with spatially dependent electronic properties. We carried out a dose test experiment to find the optimal conditions to thin-down or to cut MoS₂ flakes. The scanning step size and the exposure time have been kept fixed during the dose test (400 nm and 0.1 sec, respectively) while the laser power has been used to adjust the dose. In principle, a similar dose test can be performed by keeping fixed the laser power at an intermediate power (10 mW) and changing the exposure time to adjust the dose. However, this is limited by the minimum exposure time of our experimental setup (0.1 sec). We found that scanning step size has to be of the same order of the laser spot size in order to produce homogeneous laser thinned layers.

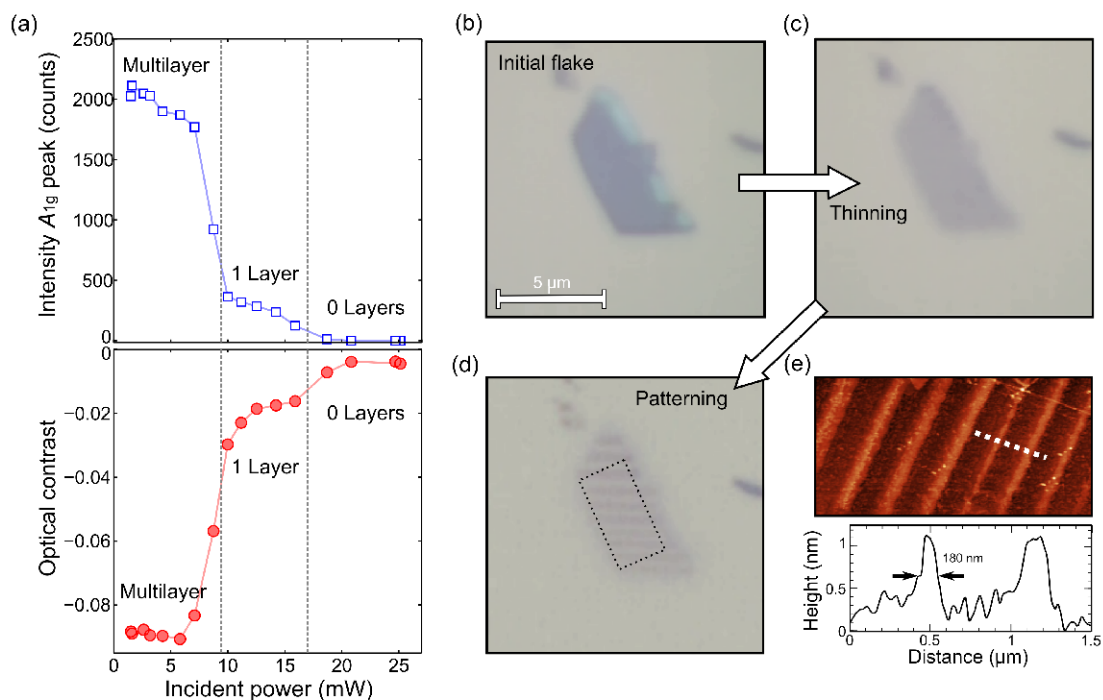


Figure 5. (a) Evolution of the optical contrast (bottom, red circles) and the intensity of the A_{1g} Raman mode (top, blue squares) as a function of the incident laser power. These signals are used to monitor the laser-thinning/cutting of MoS₂ flakes. (b,c,d) Optical images of a multi-layered MoS₂ flake at different steps during the laser-controlled thinning and patterning process: (b) initial flake, (c) after laser-thinning, (d) after patterning it into ribbons with different widths. (e) AFM topography of the single-layer MoS₂ ribbons patterned by laser.

The intensity of the A_{1g} Raman mode and the optical contrast²³, measured in a multilayered MoS₂ flake after scanning a laser with increasing power, have been employed to monitor the laser-thinning procedure. Figure 5(a) shows that while the MoS₂ flake remains unaffected for incident powers lower than 10 mW, a power between 10-17 mW (corresponding to a power density of 80-140 mW/μm²) thins down the MoS₂ flake to a single layer as can be seen from the optical contrast and the intensity of the A_{1g} Raman mode. We observed a reduction of the intensity of the A_{1g} Raman mode with the incident power (between 10 mW and 17 mW) which could be due to a degradation of the quality of the MoS₂ or to a reduction of the amount of unremoved MoS₂ traces on the surface while the power is increased. For even higher laser power, the MoS₂ layer is cut by the laser as can be inferred by the absence of the characteristic E_{2g}¹ and A_{1g} peaks in the Raman spectra and the reduced optical contrast. According to Figure 5(a), the power necessary to thin-down or to cut a multilayered MoS₂ flake is well-defined and thus it is possible to use the laser thinning to engineer the thickness and the shape of a MoS₂ flake. Figure 5(b-d) shows the different steps of the fabrication of single-layer MoS₂ ribbons of different widths by laser-thinning/cutting. The topography of the fabricated ribbons is shown in Figure 5(e); we have found that ribbons as narrow as 180 nm can be fabricated with this technique, demonstrating the power of this technique to fabricate user-defined micro/nano structures in single-layers of MoS₂.

In summary, we have developed a procedure to laser-thin multilayered MoS₂ deterministically down to a single layer in arbitrary shapes and patterns with the smallest feature size ~ 200 nm. From the analysis of their photoluminescent and electronic transport characteristics, we conclude that the semiconducting properties of the laser-fabricated monolayers resemble that of pristine MoS₂ single layers. Moreover, adjusting the laser power this technique can be employed to reliably thin or cut multilayered MoS₂ flakes, paving the way to "on demand" fabrication of MoS₂ single layers in geometries useful for future electronic, photovoltaic and optoelectronic devices.

ACKNOWLEDGMENT

This work was supported by the European Union (FP7) through the program RODIN and the Dutch organization for Fundamental Research on Matter (FOM).

REFERENCES

- (1) Novoselov, K.; Jiang, D.; Schedin, F.; Booth, T.; Khotkevich, V.; Morozov, S.; Geim, A. *Proceedings of the National Academy of Sciences of the United States of America* **2005**, 102, (30), 10451-10453.
- (2) Lee, C.; Wei, X.; Kysar, J. W.; Hone, J. *Science* **2008**, 321, (5887), 385-388.
- (3) Novoselov, K.; Geim, A.; Morozov, S.; Jiang, D.; Grigorieva, M. I. K. I. V.; Dubonos, S.; Firsov, A. *Nature* **2005**, 438, (7065), 197-200.
- (4) Coleman, J. N.; Lotya, M.; O'Neill, A.; Bergin, S. D.; King, P. J.; Khan, U.; Young, K.; Gaucher, A.; De, S.; Smith, R. J. *Science* **2011**, 331, (6017), 568-571.
- (5) Dean, C.; Young, A.; Meric, I.; Lee, C.; Wang, L.; Sorgenfrei, S.; Watanabe, K.; Taniguchi, T.; Kim, P.; Shepard, K. *Nature Nanotech.* **2010**, 5, (10), 722-726.
- (6) Steinberg, H.; Gardner, D. R.; Lee, Y. S.; Jarillo-Herrero, P. *Nano Letters* **2010**, 10, (12), 5032-5036.
- (7) Teweldebrhan, D.; Goyal, V.; Balandin, A. A. *Nano Letters* **2010**, 10, (4), 1209-1218.
- (8) Castellanos-Gomez, A.; Wojtaszek, M.; Tombros, N.; Agraït, N.; van Wees, B. J.; Rubio - Bollinger, G. *Small* **2011**, 7, (17), 2491-2497.
- (9) Ayari, A.; Cobas, E.; Ogundadegbe, O.; Fuhrer, M. S. *Journal of Applied Physics* **2007**, 101, (1), 014507.
- (10) Mak, K. F.; Lee, C.; Hone, J.; Shan, J.; Heinz, T. F. *Physical Review Letters* **2010**, 105, (13), 136805.
- (11) Kuc, A.; Zibouche, N.; Heine, T. *Physical Review B* **2011**, 83, (24), 245213.
- (12) Eda, G.; Yamaguchi, H.; Voiry, D.; Fujita, T.; Chen, M.; Chhowalla, M. *Nano Letters* **2011**, 11, (12), 5111-5116.
- (13) Korn, T.; Heydrich, S.; Hirmer, M.; Schmutzler, J.; Schüller, C. *Applied Physics Letters* **2011**, 99, (10), 102109.

- (14) Plechinger, G.; Schrettenbrunner, F. X.; Eroms, J.; Weiss, D.; Schüller, C.; Korn, T. *physica status solidi (RRL)-Rapid Research Letters* **2012**, 6, (3), 126-128.
- (15) Splendiani, A.; Sun, L.; Zhang, Y.; Li, T.; Kim, J.; Chim, C. Y.; Galli, G.; Wang, F. *Nano Lett.* **2010**, 10, (4), 1271-1275.
- (16) Radisavljevic, B.; Radenovic, A.; Brivio, J.; Giacometti, V.; Kis, A. *Nature Nanotechnology* **2011**, 6, (3), 147-150.
- (17) Li, H.; Yin, Z.; He, Q.; Li, H.; Huang, X.; Lu, G.; Fam, D. W. H.; Tok, A. I. Y.; Zhang, Q.; Zhang, H. *Small* **2012**, 8, (1), 63-67.
- (18) Radisavljevic, B.; Whitwick, M. B.; Kis, A. *ACS Nano* **2011**, 5, (12), 9934-9938.
- (19) Liu, H.; Ye, P. D. *IEEE Electron Device Letters* **2012**, 33, (4), 546-548.
- (20) Bertolazzi, S.; Brivio, J.; Kis, A. *ACS Nano* **2011**, 5, (12), 9703-9709.
- (21) Castellanos-Gomez, A.; Poot, M.; Steele, G. A.; van der Zant, H. S. J.; Agraït, N.; Rubio-Bollinger, G. *Advanced Materials* **2012**, 24, (6), 772-775.
- (22) Smith, R. J.; King, P. J.; Lotya, M.; Wirtz, C.; Khan, U.; De, S.; O'Neill, A.; Duesberg, G. S.; Grunlan, J. C.; Moriarty, G. *Advanced Materials* **2011**, 23, (34), 3944-3948.
- (23) Castellanos-Gomez, A.; Agraït, N.; Rubio-Bollinger, G. *Appl. Phys. Lett.* **2010**, 96, (21), 213116.
- (24) Li, H.; Lu, G.; Yin, Z.; He, Q.; Zhang, Q.; Zhang, H. *Small* **2012**, 8, (5), 682-686.
- (25) Han, G. H.; Chae, S. J.; Kim, E. S.; Gu nes, F.; Lee, I. H.; Lee, S. W.; Lee, S. Y.; Lim, S. C.; Jeong, H. K.; Jeong, M. S. *ACS Nano* **2011**, 5, (1), 263-268.
- (26) Zhou, Y.; Bao, Q.; Varghese, B.; Tang, L. A. L.; Tan, C. K.; Sow, C. H.; Loh, K. P. *Advanced Materials* **2010**, 22, (1), 67-71.
- (27) Park, J.; Xiong, W.; Gao, Y.; Qian, M.; Xie, Z.; Mitchell, M.; Zhou, Y.; Han, G.; Jiang, L.; Lu, Y. *Applied Physics Letters* **2011**, 98, (12) 123109.
- (28) Liu, K.-K.; Zhang, W.; Lee, Y.H.; Lin, Y.C.; Chang, M.T.; Su, C.Y.; Chang, C.S.; Li, H.; Shi, Y.; Zhang, H.; Lai, C. S.; Li, L.J. *Nano Letters* **2012**, 12, (3), 1538-1544.
- (29) Zhan, Y.; Liu, Z.; Najmaei, S.; Ajayan, P. M.; Lou, J. *Small* **2012**, 8, (7), 966-971.
- (30) Lee, C.; Yan, H.; Brus, L. E.; Heinz, T. F.; Hone, J.; Ryu, S. *ACS Nano* **2010**, 4, (5), 2695-2700.
- (31) Najmaei, S.; Liu, Z.; Ajayan, P.; Lou, J. *Applied Physics Letters* **2012**, 100, (1), 013106.
- (32) Windom, B. C.; Sawyer, W.; Hahn, D. W. *Tribology Letters* **2011**, 42, (3), 301-310.
- (33) Yin, Z.; Li, H.; Jiang, L.; Shi, Y.; Sun, Y.; Lu, G.; Zhang, Q.; Chen, X.; Zhang, H. *ACS Nano* **2012**, 6, (1), 74-80.
- (34) Ghatak, S.; Pal, A. N.; Ghosh, A. *ACS Nano* **2011**, 5, (10), 7707-7712.

Supplementary information:

Laser-thinning of MoS₂: on demand generation of a single-layer semiconductor

*A. Castellanos-Gomez, M. Barkelid, A. M. Goossens, V. E. Calado, H. S. J. van der
Zant and G. A. Steele*

Kavli Institute of Nanoscience, Delft University of Technology, Lorentzweg 1, 2628 CJ Delft, The
Netherlands.

a.castellanosgomez@tudelft.nl

Contents:

- 1) Materials and methods**
- 2) Sample fabrication**
- 3) Scanning electron microscopy characterization**
- 4) Raman spectroscopy: probing the absence of oxide**
- 5) Electrical characteristics of all the fabricated MoS₂-based devices**

Materials and methods

We prepared MoS₂ nanosheets on Si/SiO₂ substrates by mechanical exfoliation of natural MoS₂ (SPI Supplies, 429ML-AB) with blue Nitto tape (Nitto Denko Co., SPV 224P). To ensure optical visibility of ultrathin MoS₂ layers, Si/SiO₂ wafers with a 285 nm thermally grown SiO₂ layer are used¹. We located single- and few-layer MoS₂ sheets under an optical microscope (Olympus BX 51 supplemented with an Olympus DP25 digital camera) and estimated the number of layers by their optical contrast¹.

Atomic force microscopy and Raman spectroscopy were also performed for a more accurate determination of the number of layers. An atomic force microscope (Digital Instruments MultiMode III AFM with standard cantilevers with spring constant of 40 N/m and tip curvature <10 nm) operated in the amplitude modulation mode has been used to study the topography and to determine the number of layers of MoS₂ flakes previously selected by their optical contrast. A micro-Raman spectrometer (Renishaw in via RM 2000) was used in a backscattering configuration excited with a visible laser light ($\lambda = 514$ nm) to double check the number of layers of the studied MoS₂ flakes^{2, 3}. The spectra were collected through a 100 \times objective and recorded with 1800 lines/mm grating providing the spectral resolution of ~ 1 cm⁻¹. To avoid laser-induced modification of the samples, all spectra were recorded at low power levels $P < 1$ mW⁴.

Laser-thinned monolayers have been fabricated by scanning the laser of a Renishaw in via RM 2000 micro-Raman spectrometer ($\lambda = 514$ nm) over multilayered MoS₂ flakes. The exposition dose has been controlled by adjusting the incident laser power, the step size and the exposure time. We found that 10 mW of incident power, a 400 nm step size and 0.1 sec exposure time yield reproducible laser-thinning of MoS₂ flakes with initial thicknesses of 20 layers or less. We have additionally found that snake-like scans yield more uniform thinned flakes than raster-like scans.

Photoluminescence measurements have been carried out with a homemade setup that consists of a confocal microscope with a NA = 0.8 objective illuminated by a $\lambda = 532$ nm laser beam⁵. Typical light intensities of $9.5 \cdot 10^{-5}$ μ W/nm² (75 μ W incident power and 500 nm diameter spot) are used in this work. For the scanning photoluminescence measurement (Figure 3b) the diffraction limited spot is scanned using a combination of two galvomirrors and a telecentric lens system while a photoluminescence spectrum is acquired in each pixel.

For the nanofabrication of the MoS₂ based FETs, electron-beam lithography (Vistec, EBPG5000Plus HR 100) was used to write in a 495K/950K double spun PMMA layer. A 5 nm / 50 nm titanium/gold layer was evaporated. Subsequently, the PMMA/TiAu layer was gently lifted off in chloroform. Previous to their electrical characterization, samples were annealed at 250°C for two hours in a Ar/H₂ flow (500 sccm / 100 sccm), which increased their mobility by one order of magnitude⁶. Electronic transport of the MoS₂ FETs has been characterized at room temperature under high vacuum ($<10^{-5}$ mBar) in a probe station.

In order to measure the optical contrast of MoS₂ flakes we first acquired optical micrographs with a color camera attached to the trinocular of the optical microscope of a Renishaw in via RM 2000 system. The red channel of the images have been extracted and the resulting grayscale image has been employed to calculate the optical contrast $C = (I_{\text{flake}} - I_{\text{subs}}) / (I_{\text{flake}} + I_{\text{subs}})$ where I_{flake} and I_{subs} are the intensity measured in the MoS₂ flake and the SiO₂ substrate respectively^{1, 7}.

Sample fabrication

Initial atomically thin MoS₂ flakes (1-20 layers thick) have been fabricated by mechanical exfoliation on SiO₂/Si substrates with 285 nm SiO₂ to facilitate the optical identification of ultrathin flakes¹. The topography of the selected MoS₂ flakes has been studied with atomic force microscopy (Digital Instruments MultiMode III AFM) operated in the amplitude modulation mode.

Laser-thinned monolayers have been fabricated by scanning a green laser ($\lambda = 532$ nm and 10 mW of incident power) in steps of 400 nm with an exposure time of 0.1 sec between steps over multilayered MoS₂ flakes. Original flakes can be as thick as ~12 nm (20 layers). Thicker flakes cannot be easily thinned, probably because they sink the heat in a more efficient way than ultrathin flakes. Figure S1 shows the sharp profile of the step between the pristine and the laser-thinned area in a multilayered MoS₂ flake. About 9 layers have been removed by the laser.

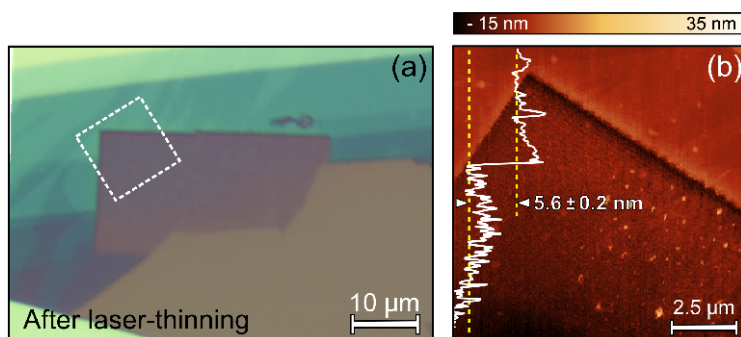


Figure S1: (a) Optical microscopy image of a multilayered MoS₂ flake deposited onto a 285 nm SiO₂/Si substrate after the laser thinning. (b) AFM topography of the region marked by the dashed square in (a). The boundary between the thinned and the pristine regions is shown. A topographic line profile shows the sharpness of the step between the thinned and pristine zones.

Figure S2 shows optical micrographs of several multilayered MoS₂ flakes before and after the laser thinning procedure. The initial thickness of the different flakes is very different as can be deduced from the diversity of optical contrast.

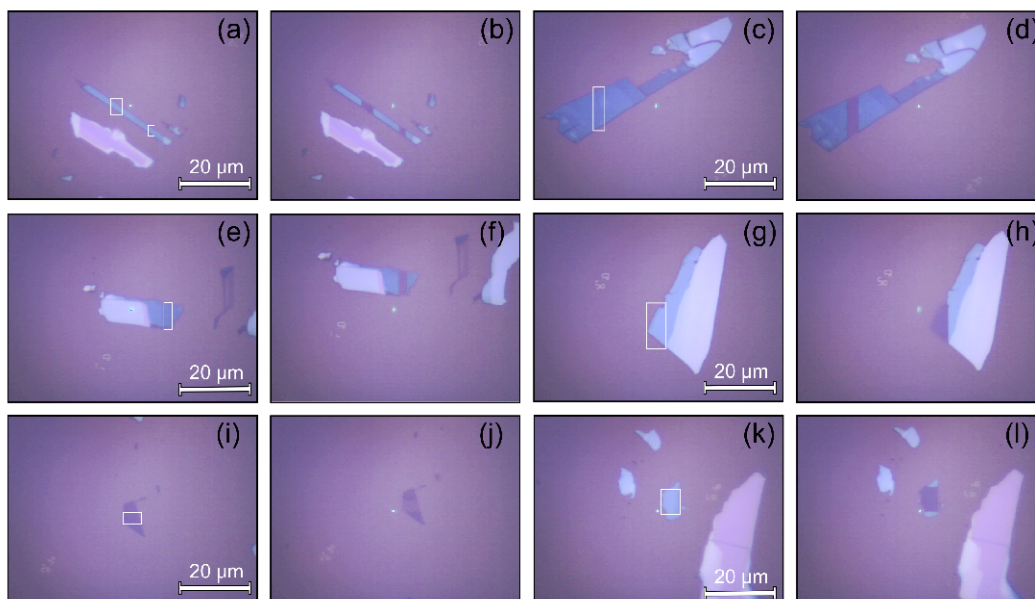


Figure S2: (a)/(b), (c)/(d), (e)/(f), (g)/(h), (i)/(j) and (k)/(l) are optical micrographs before/after thinning the regions marked by a white dotted rectangle.

Scanning electron microscopy characterization

Laser-fabricated MoS₂ monolayers (Figure S3(a)) have been additionally characterized by scanning electron microscopy with an Hitachi ultra-high resolution FE-SEM (S-4800) (see Figure S3(b)). The laser-thinned region of the MoS₂ flake present a strong difference in contrast with respect to the SiO₂, indicating that the layer is conductive, as verified by the photoluminescence and electronic transport measurements shown in the manuscript.

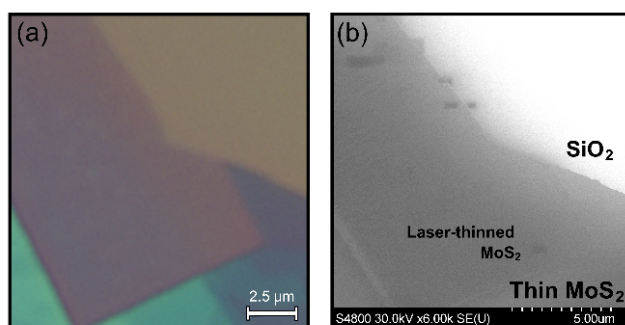


Figure S3: (a) Optical micrograph of the thinned MoS₂ flake shown in Figure 1(b) of the manuscript. (b) SEM image of the same region shown in (a).

Raman spectroscopy: probing the absence of oxide

In a recent work by Windom *et al.*⁸ they studied the oxidation of MoS₂ and its fingerprints in the Raman spectra. In that work they demonstrated that MoS₂ is oxidized in presence of pure oxygen and high temperature and they showed that this process can be monitored by means of the presence of a peak at 820 cm⁻¹ related with the presence of MoO₃ on the surface.

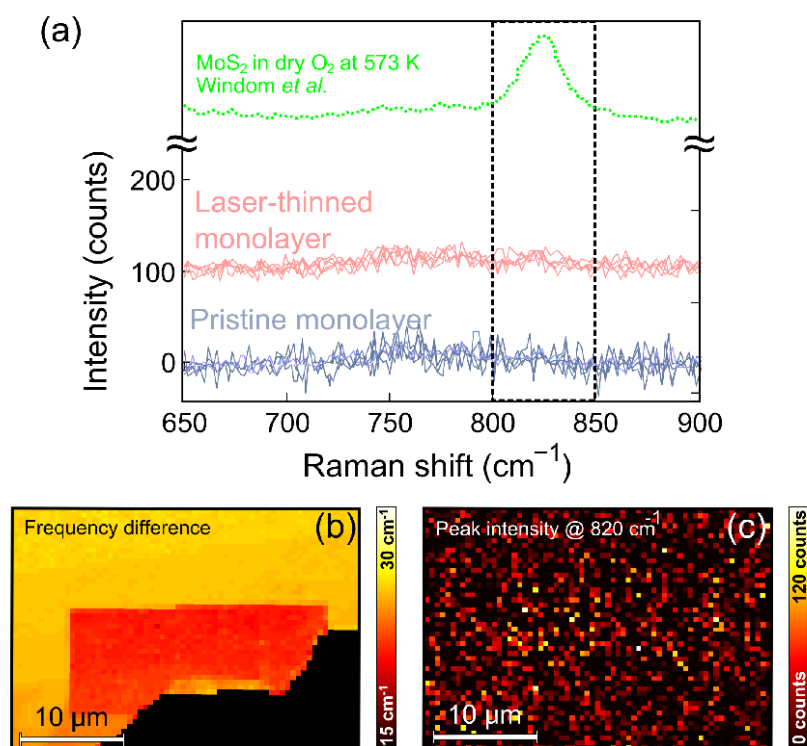


Figure S4: (a) Raman spectra of pristine and a laser-thinned MoS₂ monolayer, between 650 cm⁻¹ and 900 cm⁻¹, to probe whether the surface is oxidized or not. For comparison, it has been also added the Raman Spectrum reported for oxidized MoS₂ flakes in a dry O₂ environment at 573 K (from ref.⁸ by Windom *et al.*). (b) Spatial map of the frequency difference between the E_{1g} and A_{1g} modes (shown in Figure 2(d) of the manuscript). (c) Shows a spatial map of the integrated Raman spectra between 800 cm⁻¹ and 850 cm⁻¹ to demonstrate the absence of the MoO₃ peak (at 820 cm⁻¹) in the thinned region.

Figure S4 shows a comparison between the Raman spectra measured for a pristine and a laser-thinned MoS₂ monolayer in the region of the spectrum in where the MoO₃ peak may appear. In both spectra there are no evidence of the MoO₃ peak which indicate that the MoS₂ flakes are not oxidized during the laser thinning. This is clear if we compared those spectra with the one reported in ref.⁸ for MoS₂ oxidized in dry oxygen at 573 K that present a prominent peak at 820 cm⁻¹, clearly resolvable from the noise floor. Therefore, it is more probable that the process behind the laser thinning is sublimation and not burning of MoS₂ layers which would yield some MoO₃ on the surface. Figure S4(c) shows a spatial map with the integration of the Raman spectra between 800 cm⁻¹ and 850 cm⁻¹ to demonstrate the absence of the MoO₃ peak (at 820 cm⁻¹) in the thinned region.

Electrical characteristics of all the fabricated MoS₂-based devices

Characteristics of the fabricated FET devices are summarized in the following table.

Device	Pristine / Laser- thinned	L/W	Mobility (cm ² V ⁻¹ s ⁻¹)	Current on/off ratio
z2-fA-e12	Pristine	0.32	0.67	1400
z5-fA-e34	Pristine	0.46	0.37	12404
z3-fC-e12	Pristine	0.34	0.64	1987
z3-fA-e12	Pristine	0.31	0.05	2601
z3-fA-e45	Pristine	0.33	0.85	1987
z3-fB-e14	Laser-thinned	0.27	0.49	443
z3-fD-e34	Laser-thinned	0.25	0.17	2976
z3-fD-e23	Laser-thinned	0.48	0.18	440
z4-fD-e23	Laser-thinned	0.12	0.13	5347
z4-fD-e12	Laser-thinned	0.17	0.04	2097
z3-fB-e23	Laser-thinned	0.40	0.13	100

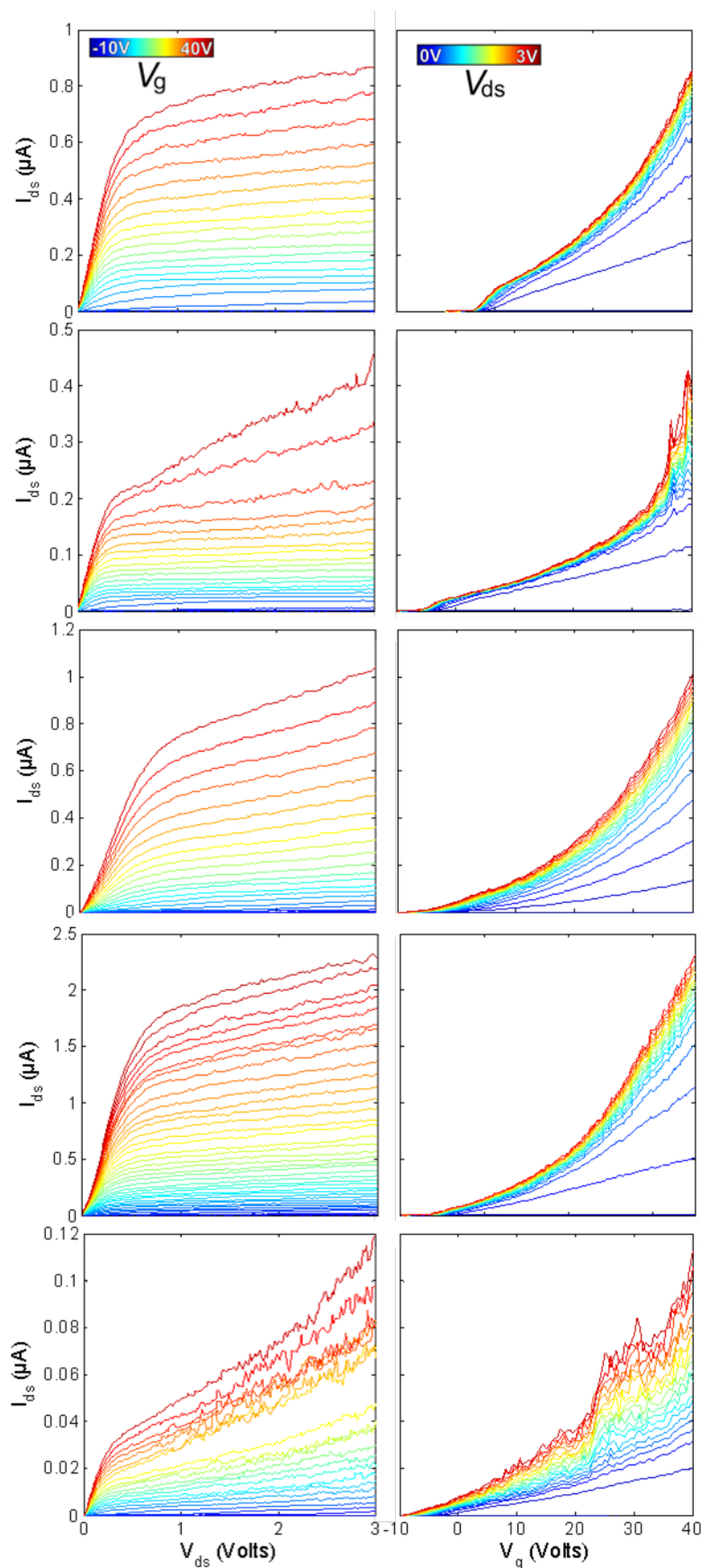


Figure S6. I_{ds} - V_{ds} and I_{ds} - V_g characteristics measured for five different FET devices based on pristine MoS₂ monolayers. The I_{ds} - V_{ds} characteristics have been measured for different gate voltages ranging from -10 V (blue traces) to +40 V (red traces). The I_{ds} - V_g characteristics have been measured for different drain source voltages ranging from -0 V (blue traces) to +3 V (red traces).

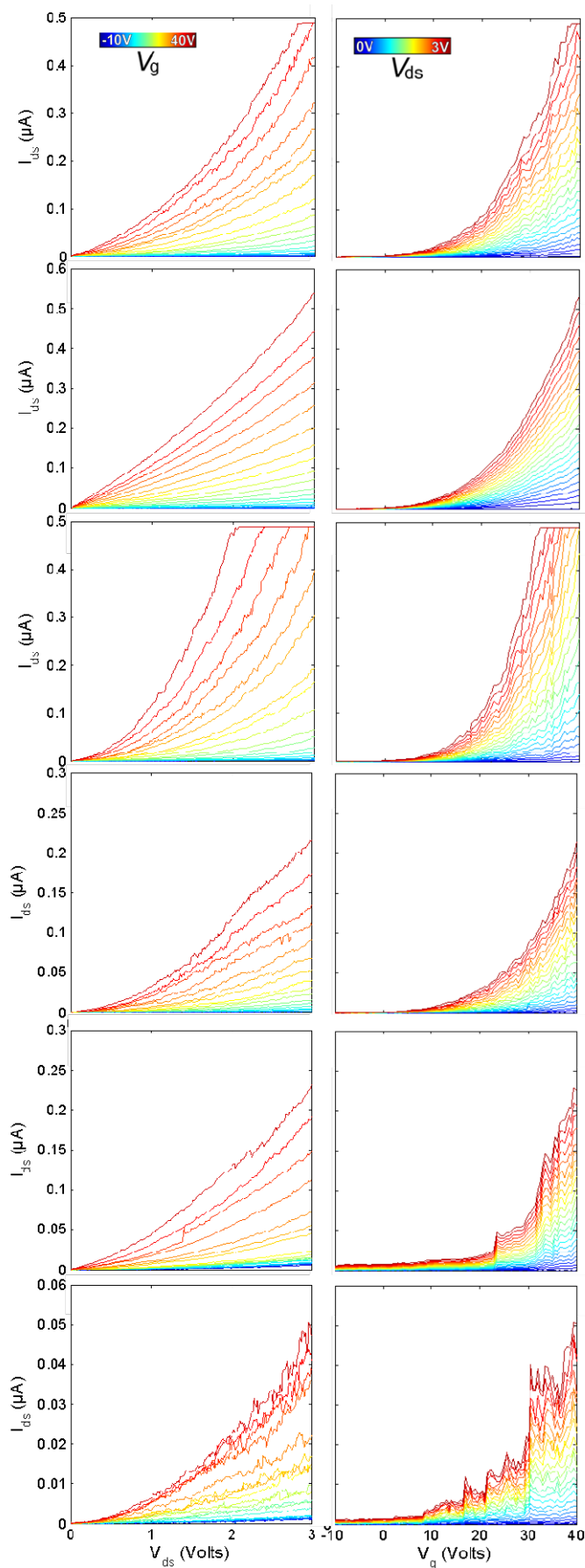


Figure S7. I_{ds} - V_{ds} and I_{ds} - V_g characteristics measured for six different FET devices based laser-fabricated MoS₂ monolayers. The I_{ds} - V_{ds} characteristics have been measured for different gate voltages ranging from -10 V (blue traces) to +40 V (red traces). The I_{ds} - V_g characteristics have been measured for different drain source voltages ranging from -0 V (blue traces) to +3 V (red traces).

References of the supplementary material

1. Castellanos-Gomez, A.; Agraït, N.; Rubio-Bollinger, G. *Applied Physics Letters* **2010**, 96, (21), 213116.
2. Lee, C.; Yan, H.; Brus, L. E.; Heinz, T. F.; Hone, J.; Ryu, S. *ACS nano* **2010**, 4, (5), 2695-2700.
3. Mak, K. F.; Lee, C.; Hone, J.; Shan, J.; Heinz, T. F. *Physical review letters* **2010**, 105, (13), 136805.
4. Najmaei, S.; Liu, Z.; Ajayan, P.; Lou, J. *Applied Physics Letters* **2012**, 100, 013106.
5. Buchs, G.; Barkelid, M.; Bagiante, S.; Steele, G. A.; Zwiller, V. *Journal of applied physics* **2011**, 110, 074308.
6. Radisavljevic, B.; Radenovic, A.; Brivio, J.; Giacometti, V.; Kis, A. *Nature Nanotechnology* **2011**, 6, (3), 147-150.
7. Li, H.; Lu, G.; Yin, Z.; He, Q.; Zhang, Q.; Zhang, H. *Small* **2012**.
8. Windom, B. C.; Sawyer, W.; Hahn, D. W. *Tribology Letters* **2011**, 1-10.